# The Vector Field Histogram—Fast Obstacle Avoidance for Mobile Robots

Johann Borenstein, *Member, IEEE*, and Yoram Koren, *Senior Member, IEEE*

*Abstract*—A new real-time obstacle avoidance method for mobile robots has been developed and implemented. This method, named the *vector field histogram* (VFH), permits the detection of unknown obstacles and avoids collisions while simultaneously steering the mobile robot toward the target.

The VFH method uses a two-dimensional Cartesian *histogram grid* as a world model. This world model is updated continuously with range data sampled by on-board range sensors. The VFH method subsequently employs a *two-stage* data-reduction process in order to compute the desired control commands for the vehicle. In the first stage the histogram grid is reduced to a one-dimensional *polar histogram* that is constructed around the robot's momentary location. Each sector in the polar histogram contains a value representing the *polar obstacle density* in that direction. In the second stage, the algorithm selects the most suitable sector from among all polar histogram sectors with a low polar obstacle density, and the steering of the robot is aligned with that direction.

Experimental results from a mobile robot traversing densely cluttered obstacle courses in smooth and continuous motion and at an average speed of 0.6–0.7 m/s demonstrate the power of the VFH method.

## I. INTRODUCTION

OBSTACLE avoidance is one of the key issues to successful applications of mobile robot systems. All mobile robots feature some kind of collision avoidance, ranging from primitive algorithms that detect an obstacle and stop the robot short of it in order to avoid a collision through sophisticated algorithms that enable the robot to detour obstacles. The latter algorithms are much more complex, since they involve not only the detection of an obstacle, but also some kind of quantitative measurements concerning the dimensions of the obstacle. Once these have been determined, the obstacle avoidance algorithm needs to steer the robot around the obstacle and proceed toward the original target. Usually, this procedure requires the robot to stop in from of the obstacle, take the measurements, and only then resume motion. Obstacle avoidance (also called reflexive obstacle avoidance or local path planning) may result in nonoptimal paths [5] since no prior knowledge about the environment is used.

A brief survey of relevant earlier obstacle avoidance methods is presented in Section II, while Section III summarizes the *virtual force field* (VFF), an obstacle-avoidance method developed earlier by our group at the University of Michigan

[5]. While the VFF method provides superior real-time obstacle avoidance for fast mobile robots, some limitations concerning fast travel among densely cluttered obstacles were identified in the course of our experimental work [18]. To overcome these limitations, we developed a new method, named *vector field histogram* (VFH), which is introduced in Section IV. The VFH method eliminates the shortcomings of the VFF method, yet retains all the advantages of its predecessor (as will be shown in Section IV). A comparison of the VFH method to earlier methods is given in Section V, and Section VI presents experimental results obtained with our VFH-controller mobile robot.

## II. SURVEY OF EARLIER OBSTACLE-AVOIDANCE METHODS

This section summarizes relevant obstacle avoidance methods, namely *edge-detection*, *certainty grids*, and *potential field methods*.

### A. Edge-Detection Methods

One popular obstacle avoidance method is based on edge-detection. In this method, an algorithm tries to determine the position of the vertical edges of the obstacle and then steer the robot around either one of the "visible" edges. The line connecting two visible edges is considered to represent one of the boundaries of the obstacle. This method was used in our very early research [4], as well as in several other works [11], [21], [22], [28], all using ultrasonic sensors for obstacle detection. A disadvantage with current implementations of this method is that the robot stops in front of obstacles to gather sensor information. However, this is not an inherent limitation of edge-detection methods; it may be possible to overcome this problem with faster computers in future implementations.

In another edge-detection approach (using ultrasonic sensors), the robot remains stationary while taking a panoramic scan of its environment [13], [14]. After the application of certain line-fitting algorithms, an edge-based *global path planner* is instituted to plan the robot's subsequent path.

A common drawback of both edge-detection approaches is their sensitivity to sensor accuracy. Ultrasonic sensors present many shortcomings in this respect:

*Poor directionality* limits the accuracy in determining the spatial position of an edge to 10–50 cm, depending on the distance to the obstacle and the angle between the obstacle surface and the acoustic axis.

*Frequent misreadings* are caused by either ultrasonic noise from external sources or stray reflections from neigh-

boring sensors (i.e., crosstalk). Misreadings cannot always be filtered out, and they cause the algorithm to falsely detect edges.

*Specular reflections* occur when the angle between the wavefront and the normal to a smooth surface is too large. In this case the surface reflects the incoming ultrasound waves away from the sensor, and the obstacle is either not detected or is "seen" as much smaller than it is in reality (since only part of the surface is detected).

Any one of these errors can cause the algorithm to determine the existence of an edge at a completely wrong location, often resulting in highly unlikely paths.

### B. The Certainty Grid for Obstacle Representation

A method for probabilistic representation of obstacles in a grid-type world model has been developed at Carnegie-Mellon University (CMU) [13], [23], [24]. This world model, called a *certainty grid*, is especially suited to the accommodation of inaccurate sensor data such as range measurements from ultrasonic sensors.

In the certainty grid, the robot's work area is represented by a two-dimensional array of square elements, denoted as cells. Each cell contains a *certainty value* (CV) that indicates the measure of confidence that an obstacle exists within the cell area. With the CMU method, CV's are updated by a probability function that takes into account the characteristics of a given sensor. Ultrasonic sensors, for example, have a conical field of view. A typical ultrasonic sensor [25] returns a radial measure of the distance to the nearest object within the cone, yet does not specify the *angular* location of the object. (Fig. 1 shows area $A$ in which an object must be located in order to result in a distance measurement $d$). If an object is detected by an ultrasonic sensor, it is *more likely* that this object is *closer* to the acoustic axis of the sensor than to the periphery of the conical field of view [4]. For this reason, CMU's probabilistic function $C_x$ increases the CV's in cells close to the acoustic axis more than the CV's in cells at the periphery.

In CMU's applications of this method [23], [24], the mobile robot remains *stationary* while it takes a panoramic scan with its 24 ultrasonic sensors. Next, the probabilistic function $C_x$ is applied to each of the 24 range readings, updating the certainty grid. Finally, the robot moves to a new location, stops, and repeats the procedure. After the robot traverses a room in this manner, the resulting certainty grid represents a fairly accurate map of the room. A global path-planning method is then employed for off-line calculations of subsequent robot paths.

### C. Potential Field Methods

The idea of imaginary forces acting on a robot has been suggested by Khatib [16]. In this method, obstacles exert repulsive forces, while the target applies an attractive force to the robot. A resultant force vector $R$, comprising the sum of a target-directed attractive force and repulsive forces from obstacles, is calculated for a given robot position. With $R$ as the *accelerating force* acting on the robot, the robot's new position for a given time interval is calculated, and the algorithm is repeated.
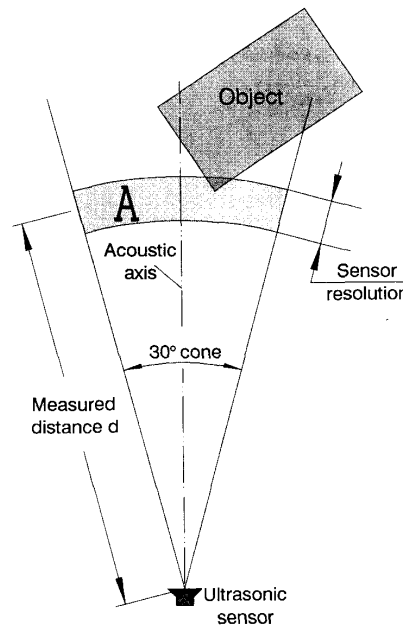


Fig. 1. Two-dimensional projection of the conical field of view of an ultrasonic sensor. A range reading $d$ indicates the existence of an object somewhere within the shaded region $A$.

Krogh [19] has enhanced this concept further by taking into consideration the robot's velocity in the vicinity of obstacles. Thorpe [27] has applied the potential field method to off-line path planning, and Krogh and Thorpe [20] suggest a combined method for global and local path planning, which uses a "generalized potential field" approach. Newman and Hogan [15] introduce the construction of potential functions through combining individual obstacle functions with logical operations.

Common to these methods is the assumption of a *known and prescribed* world model, in which simple predefined geometric shapes represent obstacles and the robot's path is generated *off-line*.

While each of the above methods features valuable refinements, none have been implemented on a mobile robot with real sensory data. By contrast, Brooks [8], [9] and Arkin [1] use a potential field method on experimental mobile robots (equipped with a ring of ultrasonic sensors). Brooks' implementation treats each ultrasonic range reading as a repulsive force vector. If the magnitude of the sum of the repulsive forces exceeds a certain threshold, the robot stops, turns in the direction of the resultant force vector, and moves on. In this implementation, however, only one set of range readings is considered, while previous readings are lost. Arkin's robot employs a similar method; his robot was able to traverse an obstacle course at 0.12 cm/s (0.4 f/s).

### III. The Virtual Force Field Method

The virtual force field (VFF) method is our *earlier* real-time obstacle avoidance method for fast-running vehicles [5].
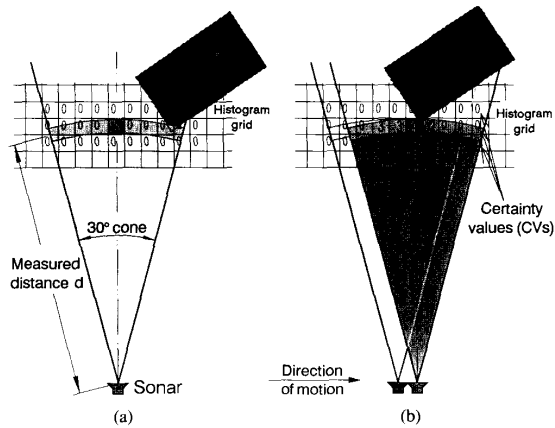
Fig. 2. (a) Only one cell is incremented for each range reading. with ultrasonic sensors, this is the cell that lies on the acoustic axis and corresponds to the measured-distance $d$. (b) A histogramic probability distribution is obtained by continuous and rapid sampling of the sensors while the vehicle is moving.
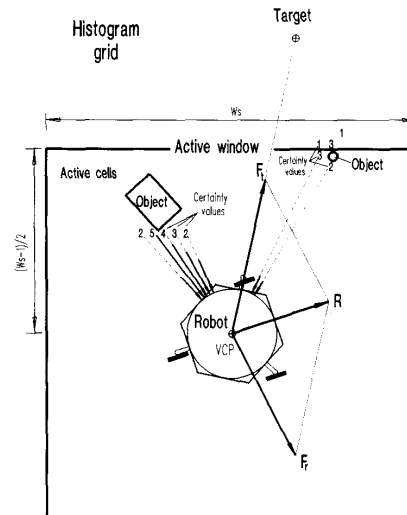


Fig. 3. The virtual force field (VFF) concept: Occupied cells exert repulsive forces onto the robot; the magnitude is proportional to the certainty value $c_{i,j}$ of the cell and inversely proportional to $d^2$.

Unlike the methods reviewed above, the VFF method allows for fast, continuous, and smooth motion of the controlled vehicle among unexpected obstacles and does not require the vehicle to stop in front of obstacles.

### A. The VFF Concept

The individual components of the VFF method are presented below.

1) The VFF method uses a two-dimensional Cartesian *histogram grid* $C$ for obstacle representation. As in CMU's certainty grid concept, each cell $(i, j)$ in the histogram grid holds a certainty value $c_{i,j}$ that represents the confidence of the algorithm in the existence of an obstacle at that location.

The histogram grid differs from the certainty grid in the way it is built and updated. CMU's method projects a probability profile onto those cells that are affected by a range reading; this procedure is computationally intensive and would impose a heavy time penalty if real-time execution on an on-board computer was attempted. Our method, on the other hand, increments only one cell in the histogram grid for each range reading, creating a "*probability*" *distribution*[1] with only small computational overhead. For ultrasonic sensors, this cell corresponds to the measured distance $d$ [see Fig. 2(a)] and lies on the acoustic axis of the sensor. While this approach may seem to be an oversimplification, a probabilistic distribution is actually obtained by continuously and rapidly sampling each sensor while the vehicle is moving. Thus, the same cell and its neighboring cells are repeatedly incremented, as shown in Fig. 2(b). This results in a *histogramic probability distribution* in which high certainty values are obtained in cells close to the actual location of the obstacle.

2) Next, we apply the potential field idea to the histogram

[1]We use the term "probability" in the literal sense of "likelihood."

grid, so the probabilistic sensor information can be used efficiently to control the vehicle. Fig. 3 shows how this algorithm works:

As the vehicle moves, a window of $w_s \times w_s$ cells accompanies it, overlying a square region of $C$. We call this region the "active region" (denoted as $C^*$), and cells that momentarily belong to the active region are called "active cells" (denoted as $c^*_{i,j}$). In our current implementation, the size of the window is 33 × 33 cells (with a cell size of 10 cm × 10 cm), and the window is always centered about the robot's position. Note that a circular window would be geometrically more appropriate, but is computationally more expensive to handle than a square one.

Each active cell exerts a *virtual repulsive force* $F_{i,j}$ toward the robot. The magnitude of this force is proportional to the certainty value $c^*_{i,j}$ and inversely proportional to $d^x$, where $d$ is the distance between the cell and the center of the vehicle, and $x$ is a positive real number (we assume $x = 2$ in the following discussion). At each iteration, all virtual repulsive forces are totaled to yield the resultant repulsive force $F_r$. Simultaneously, a virtual attractive force $F_t$ of constant magnitude is applied to the vehicle, "pulling" it toward the target. The summation of $F_r$ and $F_t$ yields the resulting force vector $R$. In order to compute $R$, up to 33 × 33 = 1089 individual repulsive force vectors $F_{i,j}$ must be computed and accumulated. The computational heart of the VFF algorithm is therefore a specially developed algorithm for the fast computation and summation of the repulsive force vectors.

3) Combining concepts 1 and 2 (given above) in real-time enables sensor data to influence the steering control *immediately*. In practice, each range reading is recorded into the histogram grid as soon as it becomes available, and the subsequent calculation of $R$ takes this data point into account. This feature gives the vehicle fast response to

obstacles that appear suddenly, resulting in fast reflexive behavior imperative at high speeds.

## B. Shortcomings of the VFF Method

The VFF method has been implemented and extensively tested on board a mobile robot equipped with a ring of 24 ultrasonic sensors (see Section VI). Under most conditions, the VFF-controlled robot performed very well. Typically, it traversed an obstacle course at an average speed of 0.5 m/s, provided the obstacles were places at least 1.8 m apart (the robot diameter is 0.8 m). With less clearance between two obstacles (e.g., a doorway), some problems were encountered. Sometimes, the robot would not pass through a doorway because the repulsive forces from both sides of the doorway resulted in a force that pushed the robot away.

Another problem arose out of the discrete nature of the histogram grid. In order to efficiently calculate repulsive forces in real time, the robot's momentary position is mapped onto the histogram grid. Whenever this position changes from one cell to another, drastic changes in the resultant $R$ may be encountered. The following numeric example explains this point. Consider a repulsive force generated by a cell $(m, n)$ and applied to the robot's momentary position at $(m, n + 6)$, which is six cells away (i.e., 0.6 m, with a cell size of $10 \times 10$ cm). The magnitude of this particular force vector is $|F_{m, n}| = k/0.6^2 = 2.8k$. As the robot advances by one cell, and its position corresponds to cell $(m, n + 5)$, the new force vector is $|F'_{m, n}| = k/0.5^2 = 4k$. The change is 42%. Changes of this magnitude cause considerable fluctuations in the steering control. The situation is even worse when the magnitude of the target-directed constant attractive force $F_t$ lies between the directions of the two successive forces $|F|$ and $|F'|$ (this condition is, in fact, most likely because it corresponds to the "steady-state" condition when the robot travels alongside an obstacle). In this situation, the direction of the resultant $R$ may fluctuate by up to 180°. For this reason it is necessary to smooth the control signal to the steering motor by adding a low-pass filter to the VFF control loop [5]. This filter, however, introduces a delay that adversely affects the robot's steering response to unexpected obstacles.

Finally, we also identified a problem that occurs when the robot travels in narrow corridors. When traveling along the centerline between the two corridor walls, the robot's motion is stable. If, however, the robot strays slightly to either side of the centerline, it experiences a strong virtual repulsive force from the closer wall. This force usually "pushes" the robot across the centerline, and the process repeats with the other wall. Under certain conditions, this process results in oscillatory and unstable motion [17], [18].

### IV. THE VECTOR FIELD HISTOGRAM METHOD

Careful analysis of the shortcomings of the VFF method reveals its inherent problem: excessively drastic data reduction occurs when the individual repulsive forces from histogram grid cells are totaled to calculate the resultant force
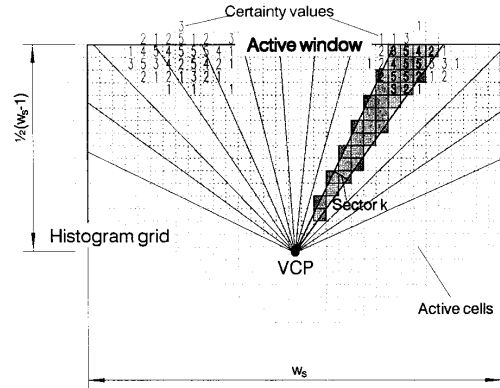


Fig. 4. Mapping of active cells onto the polar histogram.

vector $F_r$. Hundreds of data points are reduced in one step to only two items: the direction and the magnitude of $F_r$. Consequently, *detailed information about the local obstacle distribution is lost*.

To remedy this shortcoming, we have developed a new method called the *vector field histogram* (VFH). The VFH method employs a *two-stage data-reduction* technique, rather than the single-step technique used by the VFF method. Thus, three levels of data representation exist:

1) The highest level holds the detailed description of the robot's environment. In this level, the two-dimensional Cartesian histogram grid $C$ is continuously updated in real time with range data sampled by the on-board range sensors. This process is identical to the one described in Section III for the VFF method.
2) At the intermediate level, a one-dimensional *polar histogram* $H$ is constructed around the robot's momentary location. $H$ comprises $n$ angular sectors of width $\alpha$. A transformation (described in Section IV-A below) maps the active region $C^*$ onto $H$, resulting in each sector $k$ holding a value $h_k$ that represents the *polar obstacle density* in the direction that corresponds to sector $k$.
3) The lowest level of data representation is the output of the VFH algorithm: the reference values for the drive and steer controllers of the vehicle.

The following sections describe the two data-reduction stages in more detail.

### A. First Data Reduction and Creation of the Polar Histogram

The first data-reduction stage maps the active region $C^*$ of the histogram grid $C$ onto the polar histogram $H$, as follows: As with our earlier VFF method, a *window* moves with the vehicle, overlying a square region of $w_s \times w_s$ cells in the histogram grid (see Fig. 4). The contents of each active cell in the histogram grid are now treated as an *obstacle vector*, the direction of which is determined by the direction
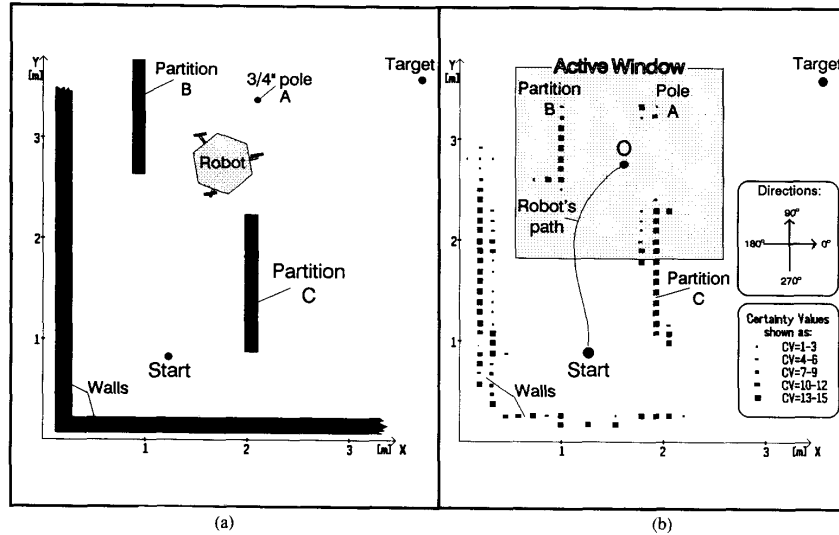
Fig. 5. (a) Example of an obstacle course. (b) The corresponding histogram grid representation.

$\beta$ from the cell to the *vehicle center point* (VCP)[2]

$$\beta_{i,j} = \tan^{-1} \frac{y_j - y_0}{x_i - x_0} \qquad (1)$$

and the magnitude is given by

$$m_{i,j} = \left(c_{i,j}^*\right)^2 (a - bd_{i,j}) \qquad (2)$$

where

| | |
|---|---|
| $a, b$ | are positive constants, |
| $c_{i,j}^*$ | is the certainty value of active cell $(i, j)$, |
| $d_{i,j}$ | is the distance between active cell $(i, j)$ and the VCP, |
| $m_{i,j}$ | is the magnitude of the obstacle vector at cell $(i, j)$, |
| $x_0, y_0$ | are the present coordinates of the VCP, |
| $x_i, y_j$ | are the coordinates of active cell $(i, j)$, and |
| $\beta_{i,j}$ | is the direction from active cell $(i, j)$ to the VCP. |

Notice that

1) $C_{i,j}^*$ is squared. This expresses our confidence that *recurring* range readings represent actual obstacles, as opposed to single occurrences of range readings, which may be caused by noise.

2) $m_{i,j}$ is proportional to $-d$. Therefore, occupied cells produce large vector magnitudes when they are in the immediate vicinity of the robot and smaller ones when they are further away. Specifically, $a$ and $b$ are chosen such that $a - bd_{max} = 0$, where $d_{max} = \sqrt{2}\,(w_s - 1)/2$ is the distance between the farthest active cell and the VCP. This way $m_{i,j} = 0$ for the farthest active cell and increases linearly for closer cells.

$H$ has a arbitrary angular resolution $\alpha$ such that $n =$

---

[2]For symmetrically shaped vehicles, the VCP is easily defined as the geometric center of the vehicle. For rectangular vehicles, it is possible to chose two VCP's, e.g., one each at the center point of the front and rear axles.

$360/\alpha$ is an integer (e.g., $\alpha = 5°$ and $n = 72$). Each sector $k$ corresponds to a discrete angle $\rho$ quantized to multiples of $\alpha$, such that $\rho = k\alpha$, where $k = 0, 1, 2, \cdots, n - 1$. correspondence between $c_{i,j}^*$ and sector $k$ is established through

$$k = \text{INT}\left(\beta_{i,j}/\alpha\right). \qquad (3)$$

For each sector $k$, the polar obstacle density $h_k$ is calculated by

$$h_k = \sum_{i,j} m_{i,j}. \qquad (4)$$

Each active cell is related to a certain sector by (1) and (3). In Fig. 4, which shows the mapping from $C^*$ into $H$, all active cells related to sector $k$ have been highlighted. Note that the sector width in Fig. 4 is $\alpha = 10°$ (not $\alpha = 5°$, as in the actual algorithm) to clarify the drawing.

Because of the discrete nature of the histogram grid, the result of this mapping may appear ragged and cause errors in the selection of the steering direction (as explained in Section IV-B). Therefore, a smoothing function is applied to $H$, which is defined by

$$h'_k = \frac{h_{k-l} + 2h_{k-l+1} + \cdots + lh_k + \cdots + 2h_{k+l-1} + h_{k+1}}{2l + 1} \qquad (5)$$

where $h'_k$ is the *smoothed polar obstacle density* (POD). In our current implementation, $l = 5$ yields satisfactory smoothing results.

Fig. 5(a) shows a typical obstacle setup in our lab. Note that the gap between obstacles $B$ and $C$ is only 1.2 m and that $A$ is a thin pole of 3/4-in diameter. The histogram grid obtained after partially traversing this obstacle course is shown in Fig. 5(b). The (smoothed) polar histogram corresponding to the momentary position of the robot $O$ is shown
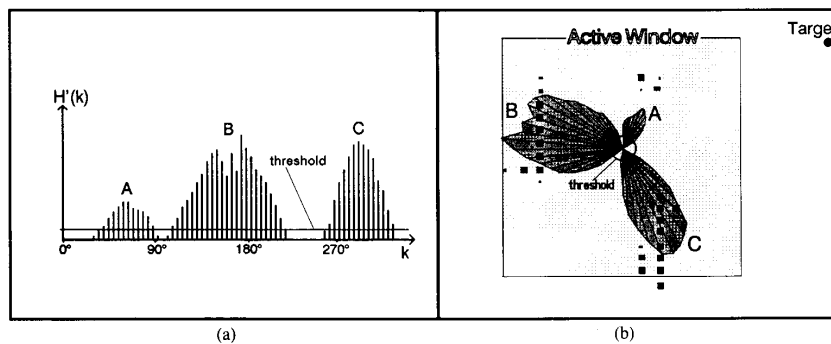
Fig. 6. (a) Polar obstacle density represented in the smoothed polar histogram $H'(k)$—relative to the robot's position at $O$ [in Fig. 5(b)]. (b) The same polar histogram as in (a), shown in polar form and overlaying part of the histogram grid of Fig. 5(b).
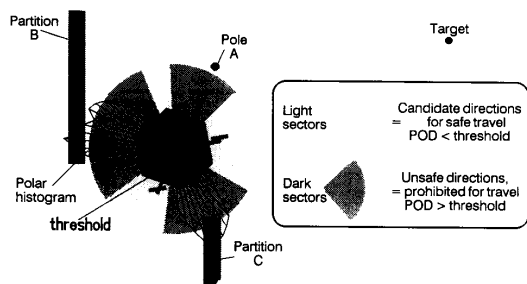


Fig. 7. A threshold on the polar histogram determines the candidate directions for subsequent travel.

in Fig. 6(a). The directions (in degrees) in the polar histogram correspond to directions measured counterclockwise from the positive $x$ axis of the histogram grid. The peaks $A, B$, and $C$ in the polar histogram result from obstacle clusters $A$, $B$, and $C$ in the histogram grid. Fig. 6(b) shows the polar form of the exact same polar histogram as Fig. 6(a), overlaying part of the histogram grid of Fig. 5(b).

### B. Second Data Reduction and Steering Control

The second data-reduction stage computes the required steering direction $\theta$. This section explains how $\theta$ is computed.

As can be seen in Fig. 6, a smoothed polar histogram typically has "peaks," i.e., sectors with high POD's, and "valleys," i.e., sectors with low POD's. Any valley comprised of sectors with POD's below a certain threshold (see discussion in Section IV-C) is called a *candidate valley*. Fig. 7 visualizes the match between candidate valleys and the actual environment: Based on the threshold and the polar histogram of Fig. 6, candidate valleys are shown as lightly shaded sectors in Fig. 7, while unsafe directions (i.e., those with POD's above the threshold) are shown in darker shades.

Usually there are two or more candidate valleys and the VFH algorithm selects the one that most closely matches the direction to the target $k_{targ}$ (an exception to this rule is discussed in Section IV-E). Once a valley is selected, it is

further necessary to choose a suitable sector *within* that valley. The following discussion explains how the algorithm finds this sector and thus the required steering direction.

At first, the algorithm measures the *size* of the *selected valley* (i.e., the number of consecutive sectors with POD's below the threshold). Here, two types of valleys are distinguished, namely, *wide* and *narrow* ones. A valley is considered wide if more than $s_{max}$ consecutive sectors fall below the threshold (in our system $s_{max} = 18$). Wide valleys result from wide gaps between obstacles or from situations where only one obstacle is near the vehicle. Fig. 8 shows a typical obstacle configuration that produces a wide valley. The sector that is nearest to $k_{targ}$ and below the threshold is denoted $k_n$ and represents the *near border* of the valley. The *far border* is denoted as $k_f$ and is defined as $k_f = k_n + s_{max}$. The desired steering direction $\theta$ is then defined as $\theta = (k_n + k_f)/2$. Fig. 8 demonstrates why this method results in a stable path when traveling alongside an obstacle: If the robot approaches the obstacle too closely [Fig. 8(a)], $\theta$ points away from the obstacle. If the robot is further away from the obstacle, $\theta$ allows the robot to approach the obstacle more closely [Fig. 8(b)]. Finally, when traveling at the proper distance $d_s$ from the obstacle [Fig. 8(c)], $\theta$ is parallel to the obstacle boundary and small disturbances from this parallel path are corrected as described above. Note that the distance $d_s$ is mostly determined by $s_{max}$. The larger $s_{max}$, the further the robot will keep from an obstacle, under steady-state conditions.

The second case, a narrow valley, is created when the mobile robot travels between closely spaced obstacles, as shown in Fig. 9. Here the far border $k_f$ is less than $s_{max}$ sectors apart from $k_n$. However, the direction of travel is again chosen as $\theta = (k_n + k_f)/2$ and the robot maintains a course centered between obstacles.

Note that the robot's ability to pass through narrow passages and doorways results from the ability to identify a narrow valley and to choose a centered path through that valley. This feature is made possible through the intermediate data representation in the polar histogram. Our earlier VFF method and other potential field methods, by contrast, lack this ability [18].
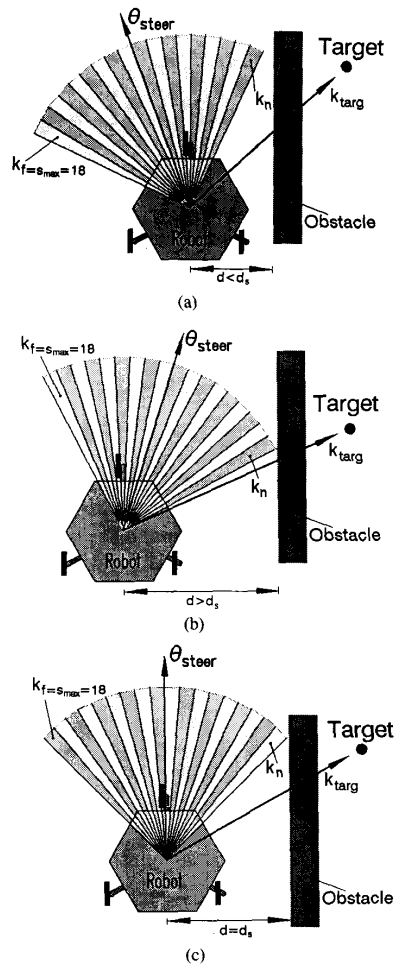
(a)

(b)

(c)

Fig. 8. Obtaining a stable path when traveling alongside an obstacle: (a) $\theta$ points away from the obstacle when the robot is too close. (b) $\theta$ points toward the obstacle when the robot is further away. (c) Robot runs alongside the obstacle when at the proper distance $d_s$.

Another important benefit from this method is the elimination of the vivacious fluctuations in the steering control (a problem associated with the VFF method). With the averaging effect of the polar histogram and the additional smoothing by (5), $k_n$ and $k_f$ (and consequently $\theta$) vary only mildly between sampling intervals. Thus, the VFH method does not require a low-pass filter in the steering control loop and is therefore able to reach much faster to unexpected obstacles. Similarly, a VFH-controlled robot does not oscillate when traveling in narrow corridors (as is the case with potential field methods, under certain circumstances [18]).

## C. The Threshold

As mentioned above, a threshold is used to determine the candidate valleys. While choosing the proper threshold is a critical issue for many sensor-based systems, the performance of the VFH method is largely insensitive to a fine-tuned threshold. This becomes apparent when considering Fig. 6:
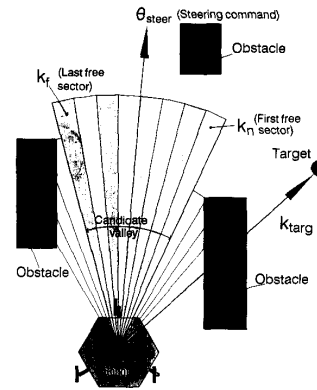


Fig. 9. Finding the steering reference direction $\theta$ when $k_{targ}$ is obstructed by an obstacle.

Lowering or raising the threshold even by a factor of 3 or 4 only affects the width of the candidate valleys. This, in turn, has only a small effect on narrow valleys, since the steering direction is chosen in the center of the valley. In wide valleys, only the distance $d_s$ from the obstacle is affected.

*Severe* maladjustments of the threshold have the following effect on the system performance:

1) If the threshold is much too large [e.g., higher than peak $A$ in Fig. 6(a)], the robot is not "aware" of that obstacle and approaches it on a collision course. However, during the approach, additional sensor readings further increase the CV's representing that obstacle, while the distance $d$ to the affected cells decreases. As is evident from (2), this results in higher POD's and consequently in a higher "peak" that *eventually* exceeds the threshold. However, in this case the robot may approach the obstacle too closely (especially when traveling at high speed) and collide with the objects.
2) If, on the other hand, the threshold is much too low, some potential candidate valleys will be precluded and the robot will not pass through narrow passages.

In summary, it can be concluded that the VFH system needs a fine-tuned threshold only for the most challenging applications (e.g., travel at high speed *and* in densely cluttered environments); under less demanding conditions, the system performs well even with an imprecisely set threshold.

One way to optimize performance is to set an *adaptive threshold* from a higher hierarchical level, e.g., as a function of a "global" plan. For example, during normal travel the threshold is set to a very safe, low level. If the global plan calls for passing through a narrow passage (e.g., a doorway), the threshold is temporarily raised while the travel speed is lowered.

## D. Speed Control

The robot's maximum speed $V_{max}$ can be set at the beginning of a run. The robot tries to maintain this speed during the run unless forced by the VFH algorithm to a lower instantaneous speed $V$, which is determined in each sampling interval as follows:

The smoothed polar obstacle density in the current direction of travel is denoted as $h'_c$. $h'_c > 0$ indicates that an obstacle lies ahead of the robot. Large values of $h'_c$ mean a large obstacle lies ahead or an obstacle is very close to the robot. Either case is likely to require a drastic change in direction, and a reduction in speed is necessary to allow the steering wheels to turn into the new direction. This reduction in speed is implemented by the following function:

$$V' = V_{\max} \left(1 - h''_c / h_m\right) \tag{6}$$

where

$$h''_c = \min\left(h'_c, h_m\right) \tag{7}$$

and $h_m$ is an empirically determined constant that causes a sufficient reduction in speed. Note that (7) guarantees $V' \geq 0$, since $h''_c \leq h_m$.

While (6) and (7) reduce the speed of the robot in *anticipation* of a steering maneuver, speed can be further reduced proportionally to the actual steering rate $\Omega$:

$$V = V'\left(1 - \Omega/\Omega_{\max}\right) + V_{\min} \tag{8}$$

where $\Omega_{\max}$ is the maximal allowable steering rate for the mobile robot (in our system $\Omega_{\max} = 120°/s$).

Note that $V$ is prevented from going to zero be setting a lower limit for $V$, namely $V \geq V_{\min}$; in our implementation $V_{\min} = 4$ cm/s.

### E. Limitations and Remedies

The VFH method is a *local path planner*, i.e., it does not attempt to find an *optimal path* (an optimal path can only be found if complete environmental information is given). Furthermore, a VFH-controlled robot may get "trapped" in dead-end situations (as is the case with other local path planners). When trapped, mobile robots usually exhibit what has been called "cyclic behavior," i.e., going around in circles or cycling between multiple traps (typical examples for cyclic behavior are discussed in [5]). While it is possible to devise a set of heuristic rules that would guide the robot our of trap situations and resolve cyclic behavior [5], the resulting path is still not optimal.

To resolve these problems, we have introduces a *path monitor* that works as follows: If the robot diverts from the target direction $k_{\text{targ}}$ (see Fig. 9) the path monitor records this as either left (as is the case in Fig. 9) or right diversion mode. Subsequently, when looking for the near border of the closest candidate valley, $k_n$ (see Section IV-B), the VFH algorithm searches to the left or right of $k_{\text{targ}}$, according to the original diversion mode. If $k_n$ cannot be found within $n = 180°/\alpha = 36$ sectors, the path monitor flags a trap situation. Once a certain diversion mode has been set, it is only cleared if the robot faces again into the target direction.

When a trap situation is flagged, the robot slows down (and may come to a complete halt), while the VFH algorithm is temporarily suspended. A *global path planner* (GPP) algorithm is then invoked to plan a new path based on the available information in the histogram grid [29]. The new path comprises a set of via points that are then presented as intermediate target locations to the VFH algorithm.

The maximum travel speed of a VFH-controlled robot is limited by the sampling rate of the ultrasonic sensors and not by the computation time of the algorithm. In our system, it takes 160 ms to have all 24 ultrasonic sensors sampled and processed once. We estimate that with our current computing hardware (see Section VI) a travel speed of up to 1.5 m/s is possible if the sampling rate of the sensors could be doubled. The relationship between sampling time, the robot travel speed, the signal-to-noise ratio, and the resulting certainty values is rather complicated and cannot be treated here because of space limitations (a through discussion of this problem is given in [6] and [7]).

## V. Comparison to Earlier Methods

During our research in obstacle avoidance for mobile robots [2]–[5], we implemented and evaluated some of the methods discussed in Section II. This section compares the performance of our new VFH method to these earlier methods.

### A. Comparison to Edge-Detection Methods

The blurry and inaccurate data produced by ultrasonic sensors does not provide the sharply defined contours required by edge-detection methods. Consequently, misreadings or inaccurate range measurements may be interpreted as part of an obstacle, thereby distorting the perceived shape of the obstacle.

The VFH method, on the other hand, reacts to clusters of range readings. As soon as a range reading has been sampled, it becomes available to the steering controller (via the histogram grid) and can influence the path of the vehicle immediately. A single range reading will have only minor influence on the path, while repeated range readings in a confined area (cluster) will cause a more drastic change of direction for the vehicle.

The force field method developed by Brooks [8], [9] and the similar method developed by Arkin [1], do function in experimental real-time systems, using actual sensory data [8], [9]. However, these methods are somewhat oversimplified, since a threshold determines if an object is at a safe distance or too close. In the latter case, and because of the binary character of the threshold, the robot must stop and rotate away from the object before resuming motion. An additional shortcoming of these methods is their susceptibility to misreadings (due to ultrasonic noise, crosstalk, etc.) since they take into account only one set of range readings (one reading from each ultrasonic sensor). Consequently, misreadings and correct readings (i.e., those produced by actual obstacles) have the same weight. Therefore, a single misreading can cause the resultant force to exceed the threshold level and "scare" the robot away from a possible safe, free path. Our method, on the other hand, also takes into account past measurements by means of the histogram grid, thereby increasing the weight of recurring measurements, while minimizing the weight of randomly occurring misreadings. In addition, the smoothing function [see (5)] reduces the weight of false readings. Thus, the VFH method results in much more robust and error-resistant control. An additional advan-
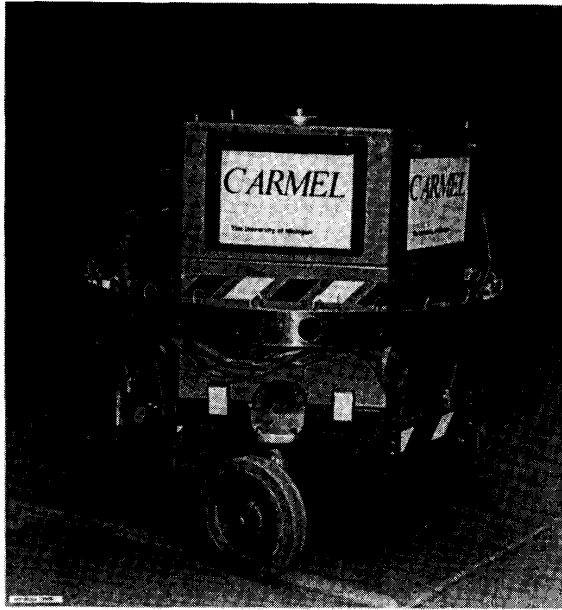
Fig. 10.   CARMEL, The University of Michigan's Mobile Robot.

tage of the VFH method is the permanent map information contained in the histogram grid after a run. Brooks' and Arkin's methods, on the other hand, do not produce a permanent record.

A critical discussion of both *simulated* and *experimental* potential field methods is given in [18]. Also, based on a rigorous mathematical analysis, [18] discusses six inherent shortcomings of potential field methods.

### B. Reflexive versus Reactive Control

On the more abstract level, researchers are beginning to distinguish between tow fundamentally different approaches to mobile robot obstacle avoidance. The "conventional" approach, *reactive* control, is based on the traditional artificial intelligence model of human cognition. Reactive control algorithms reason about the robot's perception (sensor data) while building elaborate world models (memory) and subsequently plan the robot's actions. This approach requires large amounts of computation and decision making, resulting in a relatively slow response of the system. *Reflexive* control (with Brooks as one of its foremost proponents), eliminates cognition altogether. In reflexive control there is no planning and reasoning; nor are there world models. Simple reflexes tie actions to perceptions, resulting in faster response to outside stimuli.

At first glance it may seem that our VFH method is a typical example of reactive control, considering the histogram grid world model and even a second model, the polar histogram. However, some distinctions should be made. Our world model, the histogram grid, has two different functional properties, namely a short-term effect and a long-term effect. The long-term effect is provided by the whole histogram grid, as described in Section III. The information stored in

the histogram grid may serve for map building purposes and for the global path planner (see Section IV-E). A large histogram grid, however, is not necessary for our algorithm to work properly. It is the short-term effect of the histogram grid that is important for the VFH algorithm. As explained in Section IV-A, only cells within the active window influence the VFH computations. Since the active window travels with the robot, cells are only briefly inside the window and have thus only a temporary (short term) effect. Also, since the ultrasonic sensors are limited to only 2-m look-ahead (about the size of the active window), only cells inside the window are updated with sensor information. Therefore, the VFH algorithm would work equally well if all information was lost from cells that are outside of the active window. Through the concept of the active window, the histogram grid becomes a type of "short-term memory," where readings are retained briefly (while the active window sweeps through the area) to enhance the accuracy by accumulating multiple sensor readings. In a way, this process is similar to the short-term memory associated with human hearing. Without this mechanism, people would hear but not necessarily comprehend all speech.

## VI. EXPERIMENTAL RESULTS

We implemented and tested the VFH method on our mobile robot, CARMEL (Computer-Aided Robotics for Maintenance, Emergency, and Life support). CARMEL is based on a commercially available mobile platform [12], as seen in Fig. 10. This platform has a maximum travel speed of $V_{max} = 0.78$ m/s, a maximum steering rate of $\Omega = 120°/s$, and weighs (in its current configuration) about 125 kg. The platform has a hexagonal structure and a unique three-wheel drive (synchro-drive) that permits omnidirectional steering. A Z-80 on-board computer serves as the low-level controller of the vehicle. Two computers were added: a PC-compatible single-board computer to control the sensors, and a 20-Mhz 80386-based AT-compatible that runs the VFH algorithm.

CARMEL is equipped with a ring of 24 ultrasonic sensors [25]. The sensor ring has a diameter of 0.8 m, and objects must be at least 0.27 m away from the sensors to be detected. Therefore, the theoretical minimum width for safe travel in a passageway is $W_{min} = 0.8 + 2 \cdot 0.27 = 1.34$ m.

In extensive tests, we ran the VFH-controlled CARMEL through difficult obstacle courses. The obstacles were unmarked, commonplace objects such as chairs, partitions, and bookshelves. In most experiments, CARMEL ran at its maximum speed $V_{max} = 0.78$ m/s. This speed was only reduced when an obstacle was approached head-on (see discussion of speed control in Section IV-D).

Fig. 11 shows the histogram grid after a run through a particularly challenging obstacle course of 3/4-in-diameter vertical poles spaced at a distance of about 1.4 m from each other. The actual location of the rods is indicated by plus (+) symbols in Fig. 11. It should be noted that none of the obstacle locations were known to the robot in advance: the CV clusters in Fig. 11 gradually appeared on the operator's screen while CARMEL was moving.

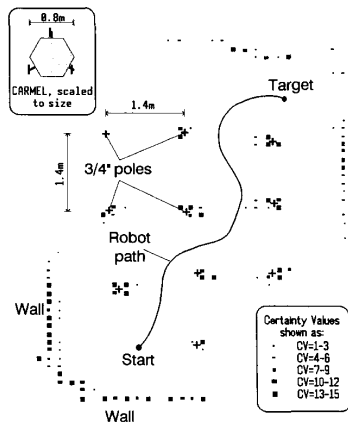To test the performance limits of our system, we per-

Fig. 11. Histogram grid representation of a run through a field of densely spaced, thin vertical poles. The average speed is this run was $V_{avrg} = 0.58$ m/s.

formed a variety of experiments with other slender obstacles. For example, 1/2-in-diameter poles were still detected, but not reliable so when approached at CARMEL's maximum speed. Unreliable detection would also result when 1 in $\times$ 1 in square rods were used. Larger objects, such as 2-in-diameter cylinders, square-shaped cardboard boxes, furniture, and even slowly walking people are reliable detected and avoided. These obstacles are easier to detect than the 3/4-in poles in the experiment described here.

Each blob in Fig. 11 represents one cell in the histogram grid. In our current implementation, certainty values (CV's) range from 0 to 15 and are indicated in Fig. 11 by blobs of varying sizes. CV = 0 means no sensor reading has been projected onto the cell during the run (i.e., no blob), while CV's > 0 indicate the increasing confidence in the existence of an object at that location. CARMEL traversed this obstacle course at an average speed of 0.58 m/s without stopping for obstacles. Note that this is a typical experimental run, and similar performance has been routinely obtained in countless experiments and demonstrations, using different kinds of obstacles at random layouts.

An indication of the real-time performance of the VFH algorithm is the sampling time $T$ (i.e., the rate at which the steer and speed commands for the low-level controller are issued). The following steps occur during $T$:

1) Obtain sonar information from the sensor controller.
2) Update the histogram grid.
3) Create the polar histogram.
4) Determine the free sector and steering direction.
5) Calculate the speed command.
6) Communicate with the low-level motion controller (send speed and steer commands and receive position update).

On an Intel 80386-based PC-compatible computer running at 20 MHz, $T = 27$ ms.

## VII. CONCLUSIONS

This paper presents a new obstacle-avoidance method for fast-running vehicles. This approach, called the vector field histogram (VFH) method, has been developed and successfully tested on our experimental mobile robot CARMEL. The VFH algorithm is computationally efficient, very robust, and insensitive to misreadings, and it allows continuous and fast motion of the mobile robot without stopping for obstacles. The VFH-controlled mobile robot traverses very densely cluttered obstacle courses at high average speeds and is able to pass through narrow openings (e.g., doorways) or negotiate narrow corridors without oscillations.

The VFH method is based on the following principles:

1) A two-dimensional Cartesian histogram grid is continuously updated in real-time with range data sampled by the on-board range sensors.
2) The histogram grid is reduced to a one-dimensional polar histogram that is constructed around the momentary location of the robot. The polar histogram is the most significant distinction between the VFF and the VFH methods as it allows a spatial interpretation (called polar obstacle density) of the robot's instantaneous environment.
3) Consecutive sectors with a polar obstacle density below threshold are called "candidate valleys." The candidate valley closest to the target direction is selected for further processing.
4) The direction of the center of the selected candidate direction is determined and the steering of the robot is aligned with that direction.
5) The speed of the robot is reduced when approaching obstacles head-on.

The characteristic behavior of a VFH-controlled mobile robot is best described as follows: The response of the vehicle is dependent on the *likelihood for the existence of an obstacle*. In the histogram grid, this likelihood is expressed in terms of size and certainty values of a cluster. This information is transformed into the height and width of an elevation in the polar histogram. The strength of the VFH method lies thus in its ability to maintain a statistical obstacle representation at both the histogram grid level as well as at the intermediate data level, the polar histogram. This feature makes the VFH method especially suited to the accommodation of inaccurate sensor data, such as that produced by ultrasonic sensors, as well as sensor fusion.

## REFERENCES

[1] R. C. Arkin, "Motor schema-based mobile robot navigation," *Int. J. Robotics Res.*, pp. 92–112, Aug. 1989.
[2] J. Borenstein and Y. Koren, "A mobile platform for nursing robots," *IEEE Trans. Industrial Electron.*, vol. 32, no. 2, pp.158–165, 1985.
[3] ——, "Motion control analysis of a mobile robot," *Trans. ASME, J. Dynamics, Measurement Control*, vol. 109, no. 2, pp. 73–79, 1987.
[4] ——, "Obstacle avoidance with ultrasonic sensors," *IEEE J. Robotics Automat.*, vol. RA-4, no. 2, pp. 213–218, 1988.
[5] ——, "Real-time obstacle avoidance for fast mobile robots," *IEEE Trans. Systems Man Cybern.*, vol. 19, no. 5, pp. 1179–1187, Sept./Oct. 1989.
[6] ——, "Histogramic in-motion mapping for mobile robot obstacle avoidance," *IEEE Trans. Robotics Automat.*, vol. 7, to be published, Aug. 1991.

[7] ——, "Real-time map-building for fast mobile robot obstacle avoidance," presented at SPIE Symp. on Advances in Intelligent Systems, Mobile Robots V, Boston, MA, Nov. 4-9, 1990.

[8] R. A. Brooks, "A robust layered control system for a mobile robot," *IEEE J. Robotics Automat.*, vol. RA-2, no. 1, pp. 14-23, 1986.

[9] R. A. Brooks and J. H. Connell, "Asynchronous distributed control system for a mobile robot," *Proc. SPIE, Mobile Robots*, vol. 727, pp. 77-84, 1987.

[10] J. L. Crowley, "Dynamic world modeling for an intelligent mobile robot," in *Proc. IEEE 7th Int. Conf. Pattern Recognition* (Montreal, Canada, July 30-Aug. 2, 1984), pp. 207-210.

[11] ——, "World modeling and position estimation for a mobile robot using ultrasonic ranging," in *Proc. IEEE Int. Conf. Robotics Automat.* (Scottsdale, AZ, May 14-19, 1989), pp. 674-680.

[12] *K2A Mobile Platform*, Cybermation, Roanoke, VA, 1987.

[13] A. Elfes, "Sonar-based real-world mapping and navigation," *IEEE J. Robotics Automat.*, vol. RA-3, no. 3, pp. 249-265, 1987.

[14] A. M. Flynn, "Combining sonar and infrared sensors for mobile robot navigation," *Int. J. Robotics Res.*, vol. 7, no. 6, pp. 5-14, Dec. 1988.

[15] W. S. Newman and N. Hogan, "High speed robot control and obstacle avoidance using dynamic potential functions," in *Proc. IEEE Int. Conf. Robotics Automat.* (Raleigh, NC, Mar. 31-Apr. 3, 1987), pp. 14-24.

[16] O. Khatib, "Real-time obstacle avoidance for manipulators and mobile robots," in *Proc. IEEE Int. Conf. Robotics Automat.* (St. Louis, MO, Mar. 25-28, 1985), pp. 500-505.

[17] Y. Koren and J. Borenstein, "Analysis of control methods for mobile robot obstacle avoidance," in *Proc. IEEE Int. Workshop Intelligent Motion Control* (Istanbul, Turkey, Aug. 20-22, 1990), pp. 457-462.

[18] ——, "Critical analysis of potential field methods for mobile robot obstacle avoidance," *IEEE Trans. Robotics Automat.*, submitted for publication.

[19] B. H. Krogh, "A generalized potential field approach to obstacle avoidance control," presented at Int. Robotics Res. Conf., Bethlehem PA, Aug. 1984.

[20] B. H. Krogh and C. E. Thorpe, "Integrated path planning and dynamic steering control for autonomous vehicles," in *Proc. IEEE Int. Conf. Robotics Automat.* (San Francisco, CA, Apr. 7-10, 1986), pp. 1664-1669.

[21] R. Kuc and B. Barshan, "Navigating vehicles through an unstructured environment with sonar," in *Proc. IEEE Int. Conf. Robotics Automat.* (Scottsdale, AZ, May 14-19, 1989), pp. 1422-1426.

[22] V. Lumelsky and T. Skewis, "A paradigm for incorporating vision in the robot navigation function," in *Proc. IEEE Conf. Robotics Automat.* (Philadelphia, PA, Apr. 25, 1988), pp. 734-739.

[23] H. P. Moravec and A. Elfes, "High resolution maps from wide angle sonar," in *Proc. IEEE Conf. Robotics Automat.* (Washington, DC), 1985, pp. 116-121.

[24] H. P. Moravec, "Sensor fusion in certainty grids for mobile robots," AI Mag., pp. 61-74, Summer 1988.

[25] POLAROID Corporation, Ultrasonic Components Group, Cambridge, MA, 1990.

[26] U. Raschke and J. Borenstein, "A comparisson of grid-type map-building techniques by index of performance," in *Proc. IEEE Int. Conf. Robotics Automat.* (Cincinnati, OH, May 13-18, 1990).

[27] C. F. Thorpe, "Path relaxation: Path planning for a mobile robot," Carnegie-Mellon Univ. The Robotics Institute, Mobile Robots Lab., Autonomous Mobile Robots, Annual Rep., pp. 39-42, 1985.

[28] C. R. Weisbin, G. de Saussure, and D. Kammer, "SELF-CONTROLLED. A real-time expert system for an autonomous mobile robot," *Computers Mechanic. Eng.*, pp. 12-19, Sept. 1986.

[29] Y. Zhao, S. L. BeMent, and J. Borenstein, "Dynamic path planning for mobile robot real-time navigation," presented at 12th IASTED Int. Symp. Robotics and Manufacturing, Santa Barbara, CA, Nov. 13-15, 1989.

**Johann Borenstein** (M'88) received the B.Sc., M.Sc., and D.Sc. degrees in mechanical engineering in 1981, 1983, and 1987, respectively, from the Technion—Israel Institute of Technology, Haifa, Israel.

Since 1987, he has been with the Robotics Systems Division at the University of Michigan, Ann Arbor, where he is currently an Assistant Research Scientist and Head of the MEAM Mobile Robotics Laboratory. His research interest include mobile robot navigation, obstacle avoidance, path planning, real-time control, sensors for robotic applications, multisensor integration, and computer interfacing and integration.

**Yoram Koren** (M'76-SM'88) has 25 years of research, teaching, and consulting experience in the automated manufacturing field. At present he is a Professor in the Department of Mechanical Engineering and Applied Mechanics at the University of Michigan, Ann Arbor. He has published over 100 papers and three books on machine tool control, robotics, sensing methods, and modeling of processes. His book *Computer Control for Manufacturing Systems* (McGraw-Hill, 1983) is used as a textbook at major universities and received the 1984 Textbook Award for the Society of Manufacturing Engineering (SME). His book, *Robotics for Engineers* (McGraw-Hill, 1985), was translated into Japanese and French and is used by engineers throughout the world.

Prof. Koren is a Fellow of the ASME, an Active Member of CIRP, and a Fellow of SME/Robotics-International.